

# Characterization of the Heavy Metal Pyrochlore Lattice Superconductor $\text{CaIr}_2$

Neel Haldolaarachchige, Quinn Gibson, Leslie M. Schoop, Huixia Luo and R. J. Cava  
*Department of Chemistry, Princeton University, Princeton, New Jersey 08544, USA*

We report the electronic properties of the cubic laves phase superconductor  $\text{CaIr}_2$  ( $T_c = 5.8$  K), in which the Ir atoms have a Pyrochlore lattice. The estimated superconducting parameters obtained from magnetization and specific heat measurements indicate that  $\text{CaIr}_2$  is a weakly coupled BCS superconductor. Electronic band structure calculations show that the Ir  $d$ -states are dominant at the Fermi level, creating a complex Fermi surface that is impacted substantially by spin orbit coupling.

## I. INTRODUCTION

Compounds based on  $5d$  transition metals are of recent interest because electron correlations and spin-orbit interactions play an important role in determining their electronic properties. Iridium oxides with the pyrochlore lattice, in particular, are predicted to host exotic electronic states<sup>1</sup>, but these materials have not yet been shown to host superconductivity. A handful of Ir compounds are known to be superconducting, some more likely showing this property due to the presence of rare earths rather than the Ir, but in other cases, such as for  $\text{IrGe}$  and  $\text{Mg}_{10}\text{Ir}_{19}\text{B}_{16}$ , the superconductivity is derived from Ir states at the Fermi Energy<sup>2-7</sup>.

Here we report the synthesis, experimental electronic characterization, and calculated electronic band structure of the cubic Laves phase superconductor  $\text{CaIr}_2$ . The Ca atoms in this material (see Fig. 1(b)) occupy the positions of the diamond structure and the Ir atoms (see Fig. 1(c)) form a pyrochlore lattice. The Ir-Ir separation in the pyrochlore network is  $2.67 \text{ \AA}$ , which is smaller than that in elemental Ir ( $2.76 \text{ \AA}$ )<sup>8</sup>. The existence of superconductivity in  $\text{CaIr}_2$  has been reported earlier, but only its  $T_c$  - no further characterization is available.<sup>9</sup> The reported  $T_c$  of  $\text{CaIr}_2$  is relatively high for an Ir-based compound, at  $5.8$  K.  $\text{CeRu}_2$ , a cubic Laves phase that we employ for comparison purposes here, displays unusual superconducting properties due to the presence of Ce  $4f$  states at the Fermi Energy.<sup>10,11</sup>

## II. EXPERIMENT AND CALCULATION

Polycrystalline samples of  $\text{CaIr}_2$  were prepared by a two-step solid state reaction method, starting from elemental Ca-pieces (99.99%; Alfa Aesar) and Ir-powder (99.99%; Alfa Aesar). A significant amount of calcium excess (200%) was found to be necessary to make high quality material due to Ca volatilization. The starting materials were added into an alumina crucible inside an Ar-filled glove box, which was then sealed inside an evacuated quartz tube. The tube was then slowly heated ( $50 \text{ }^\circ\text{C}$  per hour) and held at  $850 \text{ }^\circ\text{C}$  for 20 hrs. The resulting powder was then ground well and pressed into a pellet, again with excess calcium, slowly heated in an evacuated quartz tube to  $700 \text{ }^\circ\text{C}$ , and then held for 12 hrs.

The material was single phase at this point, and was kept inside the glove box until characterization. Such handling is necessary to avoid decomposition.<sup>12,13</sup> The purity and cell parameters of the samples were evaluated by powder X-ray diffraction (PXRD) at room temperature on a Bruker D8 FOCUS diffractometer ( $\text{Cu } K_\alpha$ ).

The electrical resistivity was measured using a standard four-probe method with an excitation current of  $10$  mA; small diameter Pt wires were attached to the sample using a conductive epoxy (Epotek H20E). Data were collected from  $300 - 2$  K and in magnetic fields up to  $5$  T using a Quantum Design Physical Property Measurement System (PPMS). The specific heat was measured between  $2$  and  $20$  K in the PPMS, using a time-relaxation method, at  $0$  and  $5$  Tesla applied magnetic fields. The magnetic susceptibility was measured in a DC field of  $10$  and  $100$  Oe; the sample was cooled down to  $2$  K in zero-field, the magnetic field was then applied, and the sample magnetization followed on heating to  $8$  K [zero-field-cooled (ZFC)], and then on cooling to  $2$  K [field-cooled (FC)] in the PPMS. The electronic structure calculations were performed by density functional theory (DFT) using the WIEN2K code with a full-potential linearized augmented plane-wave and local orbitals [FP-LAPW +  $lo$ ] basis<sup>14-17</sup> together with the PBE parameterization<sup>18</sup> of the GGA, with and without spin orbit coupling (SOC). The plane-wave cutoff parameter  $R_{MT}K_{MAX}$  was set to  $7$  and the Brillouin zone was sampled by  $20,000$  k points. The Fermi surface was plotted with the program Cryden.

## III. RESULTS AND DISCUSSION

Fig. 1 shows the PXRD analysis of the polycrystalline sample of  $\text{CaIr}_2$  employed for the characterization, the 3D crystal structure, the resistivity, and the DC-magnetization. Fig. 1(a) shows that the PXRD pattern of the  $\text{CaIr}_2$  sample is an excellent match to the standard pattern in the ICSD database (code number 108146). (The 'hump' in the low  $2\theta$  range of the PXRD pattern is due to the paratone-oil that covers the sample to prevent it from decomposing during the acquisition of the pattern.) A schematic view of the crystal structure of  $\text{CaIr}_2$  is shown in Fig. 1(d) The pyrochlore lattice of Ir atoms is emphasized.

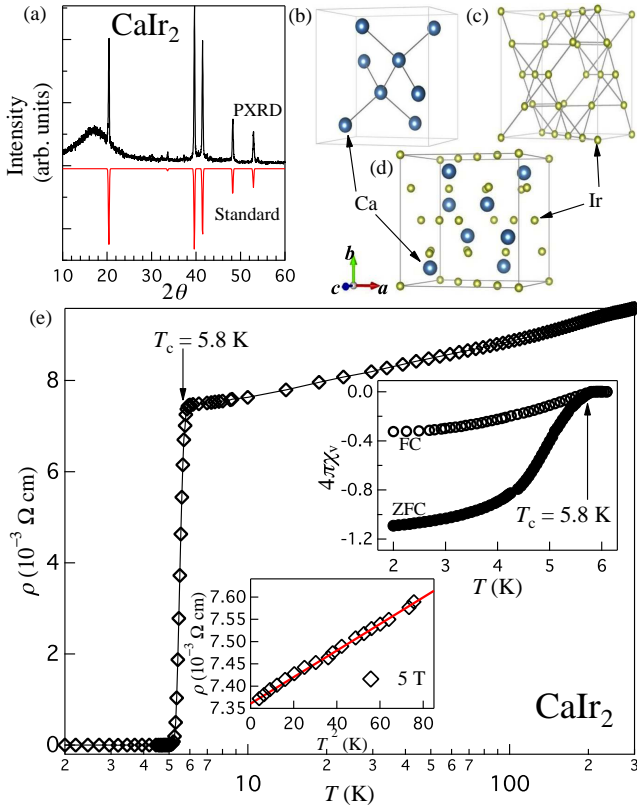


FIG. 1. (Color online) Structure and Elementary Characterization of  $\text{CaIr}_2$ . (a) the PXRD pattern of  $\text{CaIr}_2$ . (b) Represents the diamond structure for the Ca atoms  $\text{CaIr}_2$ , while (c) shows the corner sharing tetrahedral network of Ir atoms and (d) shows the full 3D crystal structure. (e) Semi log plot of resistivity as a function of temperature for  $\text{CaIr}_2$ . The upper right inset shows the DC-magnetization (ZFC and FC) as a function of temperature. The lower inset shows the resistivity as a function of  $T^2$ . The solid line in lower left inset represents a linear fit to the data.

The main panel of Fig. 1(e) shows the temperature dependent resistivity of  $\text{CaIr}_2$  from 300 to 2 K. Poor metallic behavior ( $\frac{d\rho}{dT} > 0$ ) can be observed in the normal state resistance of the polycrystalline sample, with a room temperature  $\rho \sim 9.6 \text{ m}\Omega \text{ cm}$ . A clear superconducting transition can be observed at 5.8 K. The low-temperature resistivity data (see lower left inset of the Fig. 1(e)) can be described by a power law  $\rho = \rho_0 + AT^n$  with  $n = 2$ , which follows Fermi liquid behavior. The upper right inset of the Fig. 1(e) shows the DC-magnetization of  $\text{CaIr}_2$ . The superconducting shielding can be observed in the zero-field-cooled (ZFC-shielding) and field-cooled (FC-Meissner) data in the figure. The bulk superconducting transition  $T_c^{\text{onset}} = 5.8 \text{ K}$  can clearly be observed. The very similar values of  $T_c$  seen in both resistivity and susceptibility indicates that the polycrystalline sample is nearly homogeneous.<sup>20</sup>

Fig. 2 shows the characterization of the superconduct-

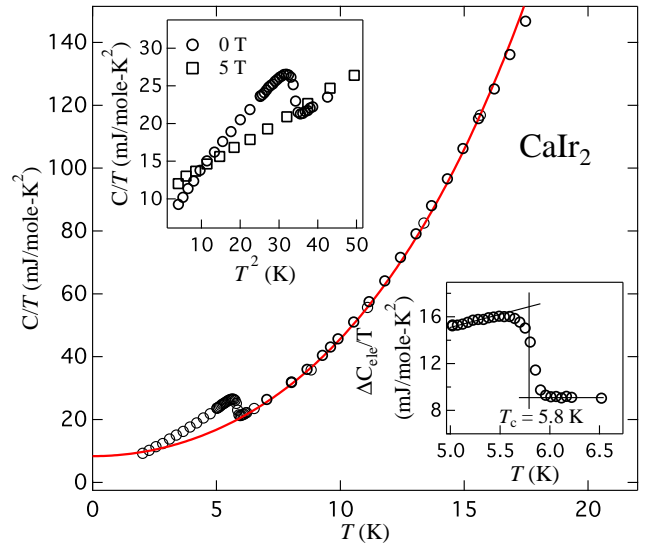


FIG. 2. (Color online) Analysis of the heat capacity of  $\text{CaIr}_2$ . (a) The main panel shows the heat capacity in 0 T applied field. The solid line shows the heat capacity data fit with the equation  $C = \gamma T + \beta_1 T^3 + \beta_2 T^5$ . The upper left inset shows the heat capacity as a function of  $T^2$  at zero applied field and 5 T applied field. The lower right inset shows the electronic heat capacity jump at  $T_c$ .

ing transition by specific heat measurements. The main panel of the Fig. 2 shows  $\frac{C}{T}$  as a function of  $T$ , characterizing the specific heat jump at the thermodynamic transition. This jump is completely suppressed under a 5 T applied magnetic field. The superconducting transition temperature  $T_c = 5.8 \text{ K}$  is shown in the lower right inset of Fig. 2, as extracted by the standard equal area construction method. The low temperature normal state specific heat is non-Debye-like. Non-Debye behavior has often been reported in superconductors and has been ascribed either to a large Einstein contribution or a low Debye temperature  $\theta_D$ . Because an Einstein phonon contribution is negligible below 20 K, a second term in the harmonic-lattice approximation is needed to improve the fit to the specific heat data. Similar behavior has been observed on some other heavy element superconductors such as  $\text{BaBi}_3$ .<sup>13</sup> We find that the low temperature normal state specific heat can be well fitted with  $\frac{C}{T} = \gamma_n + \beta_1 T^2 + \beta_2 T^4$ , where  $\gamma_n T$  represents the electronic contribution in the normal state and  $\beta_1 T^3$  and  $\beta_2 T^5$  describe the lattice-phonon contributions to the specific heat. The solid line in Fig. 2 shows the fitting; the electronic specific heat coefficient  $\gamma_n = 8.36 \frac{\text{mJ}}{\text{mol K}^2}$  and the phonon/lattice contributions  $\beta_1 = 0.32 \frac{\text{mJ}}{\text{mol K}^4}$  and  $\beta_2 = 0.00048 \frac{\text{mJ}}{\text{mol K}^4}$  are extracted from the fit. The value of  $\gamma$  obtained is smaller than that of cubic Laves phase superconductor  $\text{CeRu}_2$ , (which may be due to the fact that  $f$  orbitals are not present in the current case) but is comparable to some other alkaline/iridium based heavy element superconductors (see Table. I).<sup>6,11,12</sup>

Fig. 3 shows the analysis of the lower and upper critical fields of  $\text{CaIr}_2$ . The magnetization as a function of magnetic field over a range of temperatures below the superconducting  $T_c$  is shown in the upper right inset of Fig. 3(a). For analysis of the lower critical field, the point of 2.5% deviation from the full shielding effect was selected for each temperature. The main panel of the Fig. 3(a) shows  $\mu_0 H_{c1}$  as a function of  $T_c$ . The lower critical field behavior was analyzed with the equation  $H_{c1}(T) = H_{c1}(0) \left[ 1 - \left( \frac{T}{T_c} \right)^2 \right]$ . The  $\mu_0 H_{c1}$  data is well described with the above equation, and a least squares fit yielded the value of  $\mu_0 H_{c1}(0) = 381$  Oe, which is comparable with the cubic Laves phase  $\text{CeRu}_2$  (see Table. I).

Fig. 3(b) shows the magnetoresistance data for  $\text{CaIr}_2$ . The width of the superconducting transition increases slightly with increasing magnetic field. Selecting the 50% normal state resistivity point as the transition temperature, we estimate the orbital upper critical field,  $\mu_0 H_{c2}(0)$ , from the Werthamer-Helfand-Hohenberg (WHH) expression,  $\mu_0 H_{c2}(0) = -0.693 T_c \frac{dH_{c2}}{dT} \Big|_{T=T_c}$ . A nearly linear relationship is observed in Fig. 3(b) between  $\mu_0 H_{c2}$  and  $T_c$ . The slope is used to calculate  $\mu_0 H_{c2}(0) = 4.0$  T. This value of  $\mu_0 H_{c2}(0)$  is smaller than the weak coupling Pauli paramagnetic limit  $\mu_0 H^{Pauli} = 1.82 T_c = 10.6$  T for  $\text{CaIr}_2$ . We also used the empirical formula  $H_{c2}(T) = H_{c2}(0) \left[ 1 - \left( \frac{T}{T_c} \right)^{\frac{3}{2}} \right]^{\frac{3}{2}}$  to calculate orbital upper critical field ( $\mu_0 H_{c2}(0) = 3.8T$ ), which yields a value that agrees well with the calculated value using the WHH method. The WHH expression and the empirical formula are widely used to calculate the  $\mu_0 H_{c2}(0)$  for a variety of intermetallic and oxide superconductors.<sup>3,21-23</sup>

The upper critical field value  $\mu_0 H_{c2}(0)$  can be used to estimate the Ginzburg-Landau coherence length  $\xi(0) = \sqrt{\Phi_0 / 2\pi H_{c2}(0)} = 99$  Å, where  $\Phi_0 = \frac{hc}{2e}$  is the magnetic flux quantum.<sup>25,26</sup> This value is higher than that of the Laves phase  $\text{CeRu}_2$  (see Table. I).

The ratio  $\frac{\Delta C}{\gamma T_c}$  can be used to measure the strength of the electron-phonon coupling.<sup>27</sup> The specific heat jump  $\frac{\Delta C}{T_c}$  for the sample is about  $8 \frac{mJ}{mol K^2}$ , setting the value of  $\frac{\Delta C}{\gamma T_c}$  to 0.89. This is smaller than the weak-coupling limit of 1.43 for a conventional BCS superconductor. The results suggest that  $\text{CaIr}_2$  is a weakly electron-phonon coupled superconductor.

In a simple Debye model for the phonon contribution to the specific heat, the  $\beta$  coefficient is related to the Debye temperature  $\Theta_D$  through  $\beta = n N_A \frac{12}{5} \pi^4 R \Theta_D^{-3}$ , where  $R = 8.314 \frac{J}{mol K}$ ,  $n$  is the number of atoms per formula unit and  $N_A$  is Avogadro's number. The calculated Debye temperature for  $\text{CaIr}_2$  is thus 160 K. This value of the Debye temperature is comparable to that of  $\text{CeRu}_2$  (see Table. I). An estimation of the strength of the electron-phonon coupling can be derived from the McMillan formula  $\lambda_{ep} = \frac{1.04 + \mu^* \ln \frac{\Theta_D}{1.45 T_c}}{(1 - 0.62 \mu^*) \ln \frac{\Theta_D}{1.45 T_c} - 1.04}$ . McMillan's model

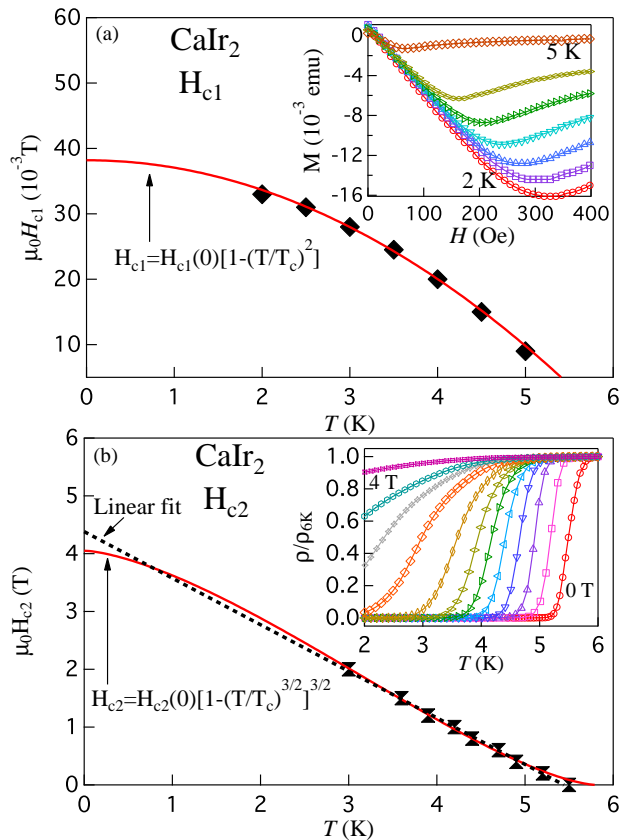


FIG. 3. (Color online) Analysis of lower and upper critical fields of the cubic Laves phase superconductor  $\text{CaIr}_2$ . (a) The lower critical field as a function of temperature. The inset shows the DC-magnetization as a function of applied magnetic field at different temperatures below the superconducting  $T_c$ . (b) The upper critical field as a function of temperature. Inset shows the resistivity with increasing applied magnetic field.

contains the dimensionless electron-phonon coupling constant  $\lambda_{ep}$ , which, in the Eliashberg theory, is related to the phonon spectrum and the density of states.<sup>28,29</sup> This parameter  $\lambda_{ep}$  represents the attractive interaction, while the second parameter  $\mu^*$  accounts for the screened Coulomb repulsion. Using the Debye temperature  $\Theta_D$ , critical temperature  $T_c$ , and making the common assumption that  $\mu^* = 0.15$ ,<sup>28</sup> the electron-phonon coupling constant ( $\lambda_{ep}$ ) obtained for  $\text{CaIr}_2$  is 0.79, which suggests weak electron-phonon coupling behavior and agrees well with  $\frac{\Delta C}{\gamma T_c} = 0.89$ .

The value of  $\gamma$  extracted from the measured specific heat data corresponds to an electronic density of states at the Fermi energy  $N(E_F)(exp)$  of 0.70 states/(eV f.u.), as estimated from the relation<sup>19,29</sup>  $3\gamma = \pi^{\frac{3}{2}} k_B^2 N(E_F)(1 + \lambda_{ep})$ . This value is slightly lower than the value obtained from our band structure calculation. The actual  $H_{c2}$  of real materials is generally influenced by both orbital and spin-paramagnetic effects. The relative importance of the orbital and spin-paramagnetic effects can be described

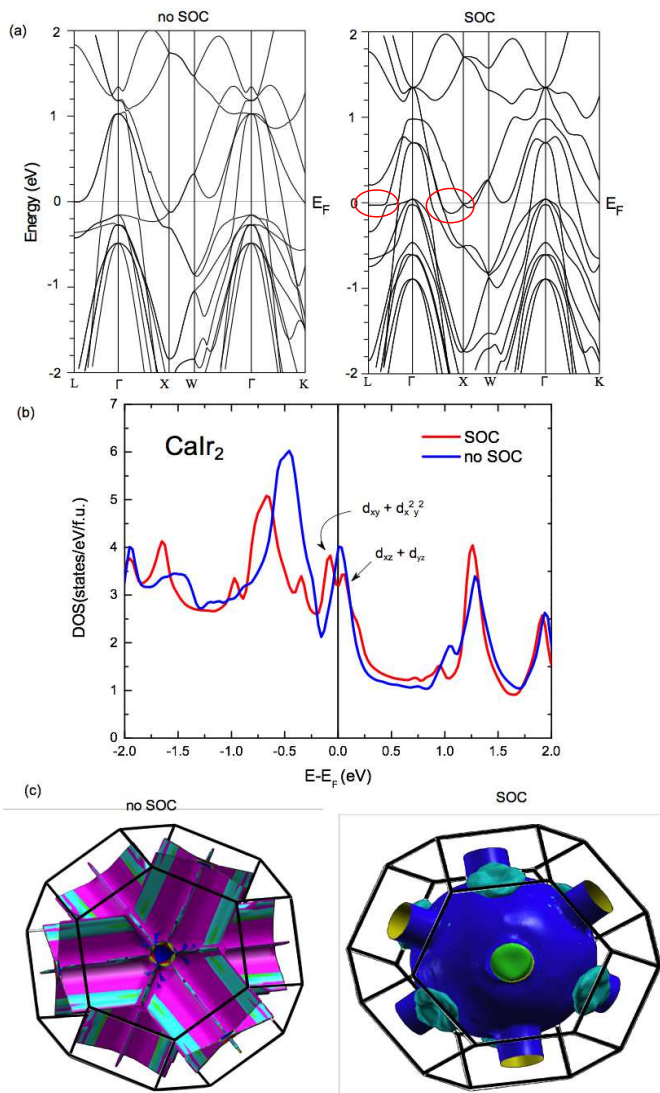


FIG. 4. (Color online) Analysis of the electronic structure of  $\text{CaIr}_2$ . (a) The electronic band structure, (b) The total DOS, and (c) the Fermi surface. The left sides of (a) and (c) show the behavior without spin orbit coupling and the right sides show the behavior with spin-orbit coupling.

by the Maki parameter,<sup>31</sup> which can be calculated as  $\frac{\mu_0 H_{c2}}{H_{Pauli}} = \frac{\alpha}{1.41} = 0.52$ .<sup>24,30,32</sup> The small Maki parameter obtained from this approximation is an indication that Pauli limiting is negligible. In contrast, a sizable Maki parameter is observed for  $\text{CeRu}_2$ , which suggests that a substantial spin-orbit component is present. Similar behavior was observed in some other unconventional superconductors such as  $\text{Nb}_{0.18}\text{Re}_{0.82}$ .<sup>21</sup> The superconducting parameters of  $\text{CaIr}_2$  are presented in Table. I. Comparison with  $\text{CeRu}_2$  is given because it shares the cubic Laves phase type structure with  $\text{CaIr}_2$ . The superconducting parameters of both compounds are comparable except that the  $\text{CeRu}_2$  is a strongly electron-phonon coupled superconductor.

TABLE I. Superconducting Parameters of the cubic Laves phase  $\text{CaIr}_2$ . Comparison is done with the cubic Laves phase  $\text{CeRu}_2$ . The superconducting parameters of  $\text{CeRu}_2$  are extracted from Ref. 10,11.

Parameter	Units	$\text{CaIr}_2$	$\text{CeRu}_2$
$T_c$	K	5.8	6.2
$\rho_0$	$m\Omega\text{cm}$	7.4	0.001
$\frac{dH_{c2}}{dT} _{T=T_c}$	$T K^{-1}$	-0.81	
$\mu_0 H_{c1}(0)$	Oe	381	200-400
$\mu_0 H_{c2}(0)$	T	4.0	7.4
$\mu_0 H^{Pauli}$	T	10.7	11.4
$\mu_0 H(0)$	T	0.06	0.073
$\xi(0)$	Å	90.7	67
$\lambda(0)$	Å	960	1100-1400
$\kappa(0)$	Å	10.6	19.4
$\gamma(0)$	$\frac{mJ}{\text{mol K}^2}$	8.4	29
$\frac{\Delta C}{\gamma T_c}$		0.89	2.0
$\Theta_D$	K	160	173
$\lambda_{ep}$		0.79	
$N(E_F)$	$\frac{eV}{f.u.}$	3.49	

Fig. 4 shows the analysis of the band structure of  $\text{CaIr}_2$  based on the ab-initio calculations. According to the calculated band structure,  $\text{CaIr}_2$  is a three-dimensional metal; several bands with large dispersion cross the Fermi level (Fig. 4(a)). There are a couple of new features observed in the band structure (see circled areas of Fig. 4(a)) due to spin orbit coupling (SOC). A saddle point (at  $E_F$ ) is visible along L- $\Gamma$  when SOC is present and as is band splitting along  $\Gamma$ -W. Saddle points in electronic band structures are instabilities that are known to cause materials to become magnetically ordered or superconducting.<sup>36,37</sup> The bands at the Fermi level are all derived from Ir  $5d$ -orbitals. Thus the pyrochlore arrangement of the Ir lattice, which determines the energy and dispersion of the bands from the Ir, has a significant effect on the electrons that become superconducting in  $\text{CaIr}_2$ . Similar dispersive bands from the pyrochlore lattice are observed for the  $4d$ -based cubic laves phase superconductor  $\text{BaRh}_2$ .<sup>34</sup> The partial DOS shows that the total DOS is dominated by the contributions from the Ir sublattice and that the contribution from the Ca atoms near the Fermi level is almost negligible. The total DOS (see Fig. 4(b)) shows that the Fermi level is located near the edge of a local maximum. Without spin orbit coupling (SOC) this peak is composed of degenerate Ir  $5d_{xy} + d_{x^2-y^2}$  and Ir  $5d_{xz} + d_{yz}$  orbitals. SOC splits the degeneracy; the Ir  $5d_{xy} + d_{x^2-y^2}$  states move slightly below the Fermi level and the Ir  $5d_{xz} + d_{yz}$  states move slightly above. Similar splitting is observed in oxide-based Ir pyrochlores<sup>36</sup>, however in that case the Ir  $5d$  electrons are more localized resulting in the opening of a band gap. The magnitude of the splitting is roughly 0.3 eV in both cases. The value of the DOS at  $E_F$  (SOC included) is comparable with

the value estimated from the heat capacity data. Many bands are found in  $\text{CaIr}_2$  through the Fermi energy, and therefore the calculated Fermi surface is complex. The Fermi surface is very strongly affected by the presence of the spin orbit coupling inherent to the  $5d$  element Ir, as seen in Fig. 4(c). Given the radical change in the Fermi surface due to the spin orbit coupling compared to the hypothetical case where no spin orbit coupling is present, one can speculate that  $\text{CaIr}_2$  has  $T_c$  on the high side of the Ir-based compounds due to the presence of the SOC.

When the Laves phase structure contains  $f$ -electrons then it seems to influence the electron-phonon coupling. To understand this picture we have compared the electronic band structure of the strongly coupled superconductor  $\text{CeRu}_2$ ,<sup>33,35</sup> with the  $\text{CaIr}_2$  electronic band structure. It can clearly be seen that the electronic structure of  $\text{CeRu}_2$  is quite different from the  $\text{CaIr}_2$  band structure. In  $\text{CeRu}_2$ , there are empty  $\text{Ce-}f$ -states just above the Fermi level, while some of the  $f$ -states are dispersed and hybridize mainly with Ru  $d$ -states. In contrast, there is not much Ca-Ir hybridization observed in the  $s$ - $d$ -bands in  $\text{CaIr}_2$ . Considering the band structure and the derived parameters for  $\text{CeRu}_2$ , it appears that one of the major effects of the hybridization of  $\text{Ce } f$ - $d$  and  $\text{Ce } f$  with Ru  $d$  bands is to enhance the electron-phonon coupling. This shows Laves phases are favorable for superconductivity from an electron-phonon perspective; however, in addition, the electronic band structures play an important role.

In oxide based Ir pyrochlores, the pyrochlore lattice causes magnetic frustration and complex behavior.<sup>36</sup> In the case of intermetallic  $\text{CaIr}_2$  the bands are not localized and no magnetism is observed. The compound becomes

superconducting, however, which might be linked to the special geometry of the pyrochlore lattice. Superconductivity can be often found close to instabilities, as for example van Hove singularities in the band structure.<sup>37</sup> In our case we see a peak in the Density of States at the Fermi level which indicates the proximity of an instability. This could indicate that the pyrochlore lattice might be advantageous for finding superconductors.

#### IV. CONCLUSION

We have characterized the properties of the pyrochlore lattice superconductor  $\text{CaIr}_2$ . The presence of a bulk superconducting transition with  $T_c = 5.8$  K was confirmed, and the properties of the superconductor were elucidated through magnetization and heat capacity measurements. The inferred electron-phonon coupling constant  $\lambda_{ep}$  and  $\frac{\Delta C}{\gamma T_c}$  show that  $\text{CaIr}_2$  is a weakly coupled BCS-type superconductor. The electronic band structure calculations indicate that the the Ir  $d$  states are dominant through the Fermi level. Given the profound effect of spin-orbit coupling on the calculated electronic structure, it can be argued that the value of  $T_c$ , and possibly even the existence of superconductivity at all, is due to the heavy element character imparted to this material by the Ir pyrochlore lattice.

#### V. ACKNOWLEDGMENTS

This work was supported by the Department of Energy, Division of Basic Energy Sciences, grant DE-FG02-98ER45706.

- 
- <sup>1</sup> William Witczak-Krempa, Gang Chen, Yong Baek Kim, and Leon Balents, *Annu. Rev. Condens. Matter Phys.* **05** 57-82 (2014).
- <sup>2</sup> R. Movshovich, M. Jaime, J. D. Thompson, C. Petrovic, Z. Fisk, P. G. Pagliuso, and J. L. Sarrao, *Phy. Rev. Lett.* **86**, 5152, (2007).
- <sup>3</sup> Daigorou Hirai, Mazhar N. Ali, and Robert J. Cava, *J. Phys. Soc. Jpn.* **82** 124701 (2013).
- <sup>4</sup> Fabian von Rohr, Huixia Luo, Ni Ni, Michael Worle, and Robert J. Cava, *Phy. Rev. B* **89**, 224504 (2014).
- <sup>5</sup> F. Honda, I. Bonalde, S. Yoshiuchi, Y. Hirose, T. Nakamura, K. Shimizu, R. Settai, and Y. Onuki, *Physica C Superconductivity* **470**, 543 (2010).
- <sup>6</sup> Daigorou Hirai, Rui Kawakami, Oxana V. Magdysyuk, Robert E. Dinnebier, Alexander Yaresko, and Hidenori Takagi, *Journal of the Physical Society of Japan* **83**, 103703 (2014).
- <sup>7</sup> T. Klimczuk, F. Ronning, V. Sidorov, R. J. Cava and J. D. Thompson, *Phy. Rev. Lett.* **99**, 257004 (2007).
- <sup>8</sup> A. E. Wood and V. B. Compton, *Acta Cryst.* **11**, 429 (1958).
- <sup>9</sup> B. T. Matthias and K. Corenzwit, *Physical Review* **107**, 06 (1957).
- <sup>10</sup> Hitoshi Sugawara, Hideyuki Sato, Tsuyoshi Yamazaki, Noriaki Kimura, Rikio Settai, and Yoshichika nuke, *J. Phys. Soc. Jpn.* **64**, 4849-4855 (1995).
- <sup>11</sup> A. D. Huxley, C. Paulsen, O. Laborde, J. L. Tholence, D. Sanchez, A. Junod, R. Calemczuk, *J. Phys. Condens. Matter* **5**, 7709 (1993).
- <sup>12</sup> S. K. Kushwaha, J. W. Krizan, Jun Xiong, T. Klimczuk, Q. D. Gibson, Tian Liang, N. P. Ong, R. J. Cava, *J. Phys. Condens. Matter* **26** 212201 (2014).
- <sup>13</sup> Neel Haldolaarachchige, Satya Kushwaha, Quinn Gibson and R. J. Cava, *Sup. Cond. Sci. and Tech.* **27**, 105001 (2014).
- <sup>14</sup> P. Blaha, K. Schwarz, G. Madsen, D. Kvasnicka and J. Luitz, WIEN2k, An Augmented Plane Wave + Local Orbitals Program for calculating Crystal Properties, Technische Universität Wien, Austria, (2001).
- <sup>15</sup> D. J. Singh, L. Nordstrom, *Planewaves, Pseudopotentials, and the LAPW Method*, Springer, New York, 2<sup>nd</sup> ed. (1996).

- <sup>16</sup> G. K. H. Madsen, P. Blaha, K. Schwarz, E. Sjöstedt, L. Nordström, Efficient linearization of the augmented plane-wave method, *Phys. Rev. B* **64** **19**, 195134 (2001).
- <sup>17</sup> E. Sjöstedt, L. Nordström, D. J. Singh, An alternative way of linearizing the augmented plane-wave method, *Solid State Communications* **114**15-20 (2000).
- <sup>18</sup> J. P. Perdew, K. Burke and M. Ernzerhof, *Phys Rev Lett.* **77**, 3865 (1996).
- <sup>19</sup> Charles Kittel, *Introduction to Solid State Physics*, Seventh Edition, John Wiley and Sons, Inc. New York (1996).
- <sup>20</sup> M. Tinkham, *Introduction to Superconductivity*, 2nd ed. McGraw Hill, New York (1975).
- <sup>21</sup> A. B. Karki, Y. M. Xiong, N. Haldolaarachchige, W. A. Phelan, Julia Y. Chan, S. Stadler, I. Vekhter, P. W. Adams, and D. P. Young, *Phys. Rev. B*, **83**, 144525 (2011).
- <sup>22</sup> Neel Haldolaarachchige, Quinn Gibson, Jason Krizan, and R. J. Cava, *Phy. Rev. B* **89**, 104520 (2014).
- <sup>23</sup> M. D. Lan, J. C. Chang, K. T. Lu, C. Y. Lee, H. Y. Shih, and G. Y. Jeng, *IEEE Transaction on Applied Superconductivity*, **11**, 3607-3610 (2001).
- <sup>24</sup> J. P. Carbotte, *Rev. Mod. Phys.* **62**, 1027 (1990).
- <sup>25</sup> N. R. Werthamer, E. Helfand and P. C. Hohenberg, *Phys. Rev.* **147**, 295 (1966).
- <sup>26</sup> A. M. Clogston, *Phys. Rev. Lett.* **09**, 266 (1962).
- <sup>27</sup> H. Padamsee, J. E. Neighbor, and C. A. Shiffman, *J. Low Temp. Phys.* **12**, 387 (1973).
- <sup>28</sup> W. L. McMillan, *Phys. Rev.* **167**, 331 (1968).
- <sup>29</sup> *Handbook of Superconductivity*, edited by C. P. Poole Jr. (Academic Press, New York, 1999), Chap. 9, Sec. G, p. 478. 422 (2009).
- <sup>30</sup> M. Zehetmayer, M. Eisterer, J. Jun, S. M. Kazakov, J. Karpinski, A. Wisniewski, and H. W. Weber, *Physical Review B* **66**, 252505 (2002).
- <sup>31</sup> Kazumi Maki, *Physical Review* **142**, 362-369 (1966).
- <sup>32</sup> A. Junod, *Studies of High Temperature Superconductors*, edited by A. Norliker, Nova Science, New York, **19** (1996).
- <sup>33</sup> N. L. Saini, S. Agrestini, E. Amato, M. Filippi, D. Di Castro and A. Bianconi, *Phy. Rev. B* **70**, 094509 (2004).
- <sup>34</sup> R. Asokamani, G. Subramoniam and S. Mathi Jaya, *Phy. Rev. B* **44**, 2283 (1991).
- <sup>35</sup> M. Higuchi and A. Hasegawa, *J. Phy. Sco. Japan* **65**, 1302-1211 (1996).
- <sup>36</sup> Xiangang Wan, Ari M. Turner, Ashvin Vishwanath, and Sergey Y. Savrasov, *Phy. Rev. B* **83**, 205101 (2011).
- <sup>37</sup> Claudia Felser and Ram Seshadri, *J. Mater. Chem.* **09**, 459464 (1999).